ACS OMEGA

http://pubs.acs.org/journal/acsodf

Article

Elucidating the Ambient Stability and Gas Sensing Mechanism of Nickel-Decorated Phosphorene for NO_2 Detection: A First-Principles Study

Soufiane Krik,* Matteo Valt, Andrea Gaiardo, Barbara Fabbri,* Elena Spagnoli, Maria Caporali, Cesare Malagù, Pierluigi Bellutti, and Vincenzo Guidi

Cite This: *ACS Omega* 2022, 7, 9808−9817

Read Online

ACCESS | Metrics & More | Article Recommendations | Supporting Information

ABSTRACT: In the field of layered two-dimensional functional materials, black phosphorus has attracted considerable attention in many applications due to its outstanding electrical properties. It has experimentally shown superior chemical sensing performance for the room temperature detection of NO_2, highlighting high sensitivity at a ppb level. Unfortunately, pristine black phosphorus demonstrated an unstable functionality due to the fast degradation of the material when exposed to the ambient atmosphere. In the present work, a deepened investigation by density functional theory was carried out to study how nickel decoration of phosphorene can improve the stability of the material. Further, an insight into the sensing mechanism of nickel-loaded phosphorene toward NO_2 was given and compared to pristine phosphorene. This first-principles study proved that, by introducing nickel adatoms, the band gap of the material decreases and the positions of the conduction band minimum and the valence band maximum move toward each other, resulting in a drop in the conduction band minimum under the redox potential of O_2/O_2^-, which may result in a more stable material. Studying the adsorption of O_2 molecules on pristine phosphorene, we also proved that all oxygen molecules coming from the surrounding atmosphere react with phosphorus atoms in the layer, resulting in the oxidation of the material forming oxidized phosphorus species (PO_x). Instead, by introducing nickel adatoms, part of the oxygen from the surrounding atmosphere reacts with nickel atoms, resulting in a decrease of the oxidation rate of the material and in subsequent long-term stability of the device. Finally, possible reaction paths for the detection of NO_2 are given by charge transfer analyses, occurring at the surface during the adsorption of oxygen molecules and the interaction with the target gas.

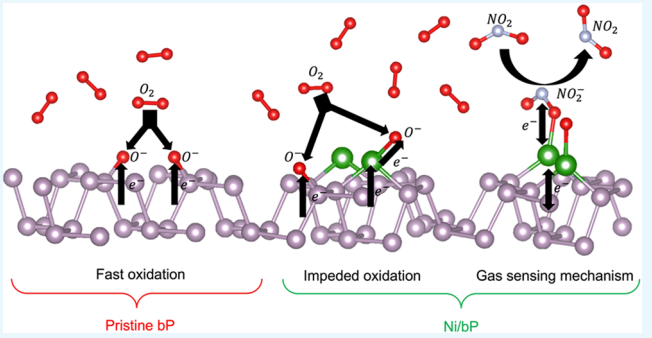

INTRODUCTION

Since its discovery,[1] graphene has been widely studied due to its excellent electronic, optical, and mechanical properties.[2−4] Then, many kinds of two-dimensional (2D) materials have attracted attention because of their quantum confinement effect, high-specific surface areas, and excellent flexibility.[5−14] The high surface-to-volume ratio and low electrical noise made them interesting materials with a great potential in many technological applications including gas sensing,[15−20] in which metal-oxide semiconductors are the most widely investigated materials.[21−29] However, the gapless characteristic of graphene limits its applications, inspiring researchers to investigate other 2D materials, which possess similar properties with a suitable band gap.

Phosphorene is an innovative 2D material, whose band gap, electronic structures, and reactivity can vary according to the number of layers, surface defects, doping, and configurations of its films.[30,31] Among the allotropes of phosphorus, including the groups of red, white, and violet phosphorus,[32] black phosphorus (bP) is the most stable. The successful fabrication of exfoliated bP and evaluation of its outstanding performance in field-effect transistors was reported in 2014[33,34] and paved the way to the practical use of bP in electronic sensing devices. Indeed, these works have shown that small molecules such as CO, H_2, H_2O, NH_3, NO, and NO_2 are physisorbed on phosphorene with high adsorption energies, even higher than other 2D materials, such as graphene and MoS_2,[31] suggesting its use as a high-performance chemical sensor.

New studies on phosphorene modifications highlighted that its operation stability and sensitivity can be improved by different passivation strategies, such as doping and composite formation with metal oxides,[35,36] noble metals,[37] polymers,[38] or

Received: January 5, 2022
Accepted: February 28, 2022
Published: March 10, 2022

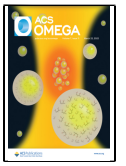

metal−organic frameworks.[39] In particular, bP modifications by adatom doping, including transition metals and nonmetallic atoms, e.g., S, Si, O, Ge, can tune the material band gap and electronic properties. Lalitha et al.[40] demonstrated that the addition of calcium to bP can improve the adsorption of gaseous molecules on the surface of pristine phosphorene. Li et al.[41] studied the adsorption of H_2 on Li-doped phosphorene and reached a similar conclusion. Caporali et al.[42] experimentally demonstrated the ambient stability and functionality improvement of nickel-decorated bP (Ni/bP) films. As a result, nickel is a good choice for bP functionalization, as it has been shown to improve bP ambient stability. Nickel is also well-known for its gas sensing capabilities in a variety of structures and under a variety of situations.[43−46] Furthermore, first-principles simulations revealed a significant adsorption energy for Ni-decorated bP,[47] which is substantially higher than the adsorption energy of Ni adatoms on graphene,[48] implying that the functionalization is more successful. In recent studies, our research group observed an enhancement in the stability of electrical signals and sensing performance of phosphorene films after decoration with Ni, i.e., high selectivity toward NO_2 in sub-ppm concentrations at room temperature, obtained through a simple, reproducible, and affordable deposition technique.[49] The successful experimental results of decorated phosphorene made this system appealing for deepened theoretical studies.

Until now, only a few theoretical works deal with the interactions between doped phosphorene and small molecules.[50] Among the theoretical approaches employed to investigate the possible reactions occurring at the surface of a gas sensor, density functional theory (DFT) calculations represent a powerful tool to understand the physical−chemical properties of the investigated materials under different simulated environments by giving an overview at the microscopic level of the elementary steps of the reaction processes. Recently, some interesting works were published about DFT studies on gas molecule adsorption on pristine phosphorene.[51−54] Then, starting from these preliminary investigations, in the present work, a first-principles study in the framework of DFT was carried out to in-depth understanding on how nickel influences the electronic properties of bP improving its ambient stability. This study could be useful in all bP applications, where oxygen impacts the stability of the film by irreversible oxidation. Moreover, the sensing mechanism of Ni-decorated bP toward NO_2 gas was studied to theoretically support the experimental results of increased selectivity identified in our previous works.[49]

METHODOLOGY

The theoretical study was organized following these steps:

- the electronic structures and the density of states were calculated for both materials, pristine and nickel-loaded phosphorene, to understand the behavior of the impurity states created by nickel addition;
- the first step of the sensing mechanism of the decorated material was studied starting by the adsorption of oxygen from the surrounding atmosphere;
- the second step was investigated by studying the interaction with the target gas and deepening the charge transfer occurring on the surface of the film.

COMPUTATIONAL DETAILS

Different approximations and parametrizations were used to perform the calculations required for investigating the material properties and understanding the sensing mechanism.

A plane-wave pseudopotential (PWPP) approach[55] was adopted for the solution of the Kohn−Sham equations.[56] It is based on atomic pseudopotentials and a set of plane wave basis as implemented in the Quantum ESPRESSO code.[57] This approach was used since it is very efficient in dealing with extended periodic systems, such as Ni-decorated bP proposed here. The code is built on the use of periodic boundary conditions. It allows an easy treatment of infinite crystalline systems and fast convergence to the thermodynamic limit for periodic but extended systems, e.g., liquids or amorphous materials.

Periodic boundary conditions in the slab method were applied to generate a supercell with unlimited replica along the surface plane. Plane waves can be used to expand wave functions in this scenario. Furthermore, a certain number of solid slices were replicated in the perpendicular direction to recreate a real solid structure. Adsorbates must not interact with their own periodic duplicates, hence, in the perpendicular direction, a sufficient vacuum must be adjusted so that the interface resembles a real surface.

Self-consistent field (SCF) calculations were performed using generalized gradient approximation with Perdew−Burke−Ernzerhof parameterization (GGA-PBE)[58] for the exchange−correlation functional and ultrasoft pseudopotentials to represent the ion nuclei. The cutoff energies for the wave functions and charge density were optimized for the minimum total energy of the system, and the optimized values were set to 37 and 333 Ry, respectively. A high value of the charge density cutoff was needed to ensure the accurate estimation of the electrostatic potential. The $(6 \times 1 \times 4)$ Monkhorst-Pack grid[59] was set for the number of K-points in the first Brillouin zone for SCF cycles, and $(18 \times 3 \times 12)$ was used for density of states (DOS) calculations.

The convergence criteria were set for all calculations to 10^{-6} Ry for the total energy of the system and 1 mRy/Bohr for the total force acting on each atom. The relaxation method used was the Broyden_Fletcher_Goldfarb_Shanno (BFGS) algorithm.[60]

Also, to treat the van der Waals interactions, van der Waals DFT (vdW-DF) with optB88 (optB88-vdW)[61,62] was considered in this work for the exchange functional during the relaxation of the system.

RESULTS AND DISCUSSION

Before investigating the impact of decorating phosphorene with nickel, the crystal structure of bP was optimized and phosphorene was cleaved and optimized, and then decorated with nickel. The results concerning this part of the work are discussed in the Supporting Information and reported in Figures S1−S4 and Tables S1 and S2. These calculations were necessary to optimize the basic model used in this work. To study the impact of Ni adatom introduction on the physical−chemical properties of phosphorene, a Ni atom was placed in the hollow (H) site at $h = 1.01$ Å as a vertical height of the adatom from the phosphorene layer.[63] The H site was chosen since it is the most stable adsorption site for Ni. Moreover, the distance between the Ni adatom and the phosphorene layer was adopted based on the study done by Hu et al.[63] After relaxation of the system, the calculated vertical height of the nickel adatom with respect to the

https://doi.org/10.1021/acsomega.2c00078
ACS Omega 2022, 7, 9808−9817

closer phosphorus atoms was found to be 0.999 Å, which is coherent to the reported value in the literature (i.e., 1.01 Å).[63]

Impact of Nickel Adatoms on the Electronic Structure of Phosphorene. After relaxation of the system, the GGA_PBE approximation was adopted to calculate the band structure and the density of states of nickel-decorated phosphorene as previously reported in ref 38. Before going further, it is worthwhile to recall the principle of doping in semiconductors. Indeed, a semiconductor doped with ionized impurities contains free carriers. If the impurity states appear close to the top of the valence band (VB)/bottom of the conduction band (CB), they are called shallow acceptor/donor levels, respectively. On the other hand, they are called deep acceptor/donor levels if they appear close to the middle of the forbidden band gap. Shallow impurities require little energy (i.e., typically, at KT thermal energy or less) to be ionized, while the energy required for deep impurities is much greater, and only a fraction of the impurities in the semiconductor contributes to the free carriers. Therefore, deep impurities have very little chance of being ionized since they are far away from both band edges, more than five times the thermal energy. It was clear from our previous study that the considered material is a p-type semiconductor due to the appearance of a new band in the band gap region, just below the Fermi level. This new energy level acts as a shallow acceptor level since it lies between the top of the VB and below the Fermi level. The band gap calculated after Ni decoration turns out to be an indirect band gap with a value of about 0.68 eV, which is decreased by 25% from the calculated value of pristine phosphorene equal to 0.9 eV. From the DOS graph reported in ref 38, the corresponding peak of the new band created by nickel doping can be clearly seen.

The electronic configuration of phosphorus is [Ne] $3s^2 3p^3$, while the nickel one is [Ar] $3d^8 4s^2$. Before the introduction of the nickel atom, both the top of the VB and the bottom of the CB were mainly composed of states coming from the *p* orbitals of the phosphorus atoms. Due to the sp^3 hybridization of phosphorus atoms in phosphorene, adsorbates can act as an electron acceptor, facilitating the formation of bonds with P atoms exploiting the electron lone pairs on the latter. Then, in the case of pristine bP, oxygen atoms from the surrounding atmosphere react with the lone pairs of P atoms at the surface, resulting in a high oxidation rate of the material.[47] Introducing the nickel atom, hybridization of p orbitals of P and d orbitals of Ni atoms occurred. The bond between nickel and phosphorus atoms reduces the number of lone pairs on P atoms. This prevents the reaction with oxygen and leads to a decrease in the oxidation rate of the material, resulting in better stability and performance as a gas sensor.[64] For this application, the shallow acceptor level can facilitate electron exchange between the top of the VB and the target gas.[65] Thus, the increase of hole concentration on the VB may enhance the reactivity of the material surface.

To elucidate the stability and sensing improvement of Ni-decorated bP, its work function values were compared to pristine bP ones. The work function (Φ) is defined as the minimum energy needed for an electron to move from the surface to the vacuum level,[66] which can be expressed as $\Phi = V_{vac} - E_F$, where V_{vac} is the electrostatic potential in the vacuum region and E_F is the electrostatic potential at the Fermi level. The work function values were calculated for pristine and nickel-decorated phosphorene to elucidate the stability improvement of the sensor device due to an increase of the material stability. The calculated work functions of pristine and nickel-decorated phosphorene were about 4.59 and 4.49 eV, respectively. The obtained value, in the case of pristine phosphorene, is in good agreement with other reported values using the GGA_PBE approximation (i.e., 4.50 eV).[66] These values are slightly underestimated using the GGA_PBE approximation, but it still gives an accurate description of the trend.[67,68] Based on the study reported by Zhou et al.,[69] phosphorene can produce excitons under ambient light due to its large band gap. In other words, since the redox potential of O_2/O_2^- is included inside the forbidden band gap region, in the case of monolayer bP, the photogenerated electrons will pass from the bP CB to adsorbed O_2 on the surface, generating O_2^-. This might involve irreversible oxidation of the p-doped phosphorene, causing its degradation and forming oxidized phosphorus species (P_xO_y), fundamentally altering the electronic properties of phosphorene. However, Zhou et al.[69] reported that, by increasing the number of layers, the band gap decreases and both the valence band maximum (VBM) and conduction band minimum (CBM) move close to each other, until the CBM overlaps or even goes under the redox potential of O_2/O_2^-. This can improve the ambient stability of the material since, in our case, the trend of the band gap and work function, comparing pristine and nickel-decorated phosphorene, is similar to the previously reported study.[69] Therefore, it is possible to assume that, by introducing the nickel atom, the CBM shifts toward the redox potential of O_2/O_2^-, as schematized in Figure 1. Indeed, in our calculated DOS,

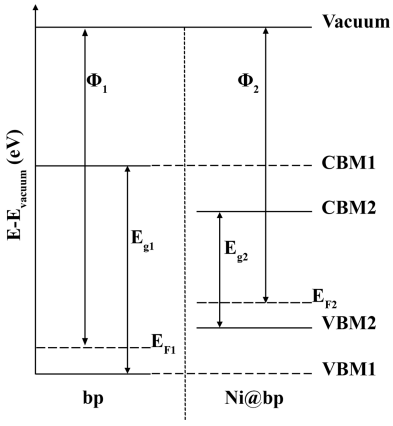

Figure 1. Scheme illustrating the movement of band level before (VBM1, CBM1, E_{F1}, E_{g1}, Φ_1) and after (VBM2, CBM2, E_{F2}, E_{g2}, Φ_2) the introduction of the nickel atom.

reported in ref 49, the movement of the top of the VB toward high energies is clearly visible as well as the CBM that slightly shifts down to low energies. Considering the applied approximation, this band movement can be considered even if it consists of a small shift. The overall conclusion from these analyses can be translated to the improved stability of the sensors fabricated using nickel-loaded phosphorene rather than the one based on pristine phosphorene.

Sensing Mechanism of Nickel-Decorated Phosphorene Toward NO_2. The reaction mechanism occurring at the film surface related to the interaction between gaseous compounds and the principle at the basis of NO_2 detection are proposed here. First, oxygen molecules from the surrounding atmosphere can be adsorbed and transformed into oxygen ions by trapping electrons located at the surface of the active material.[70] This results in a creation of a hole accumulation layer and in an increase of carrier concentration, which lowers the overall

https://doi.org/10.1021/acsomega.2c00078
ACS Omega 2022, 7, 9808−9817

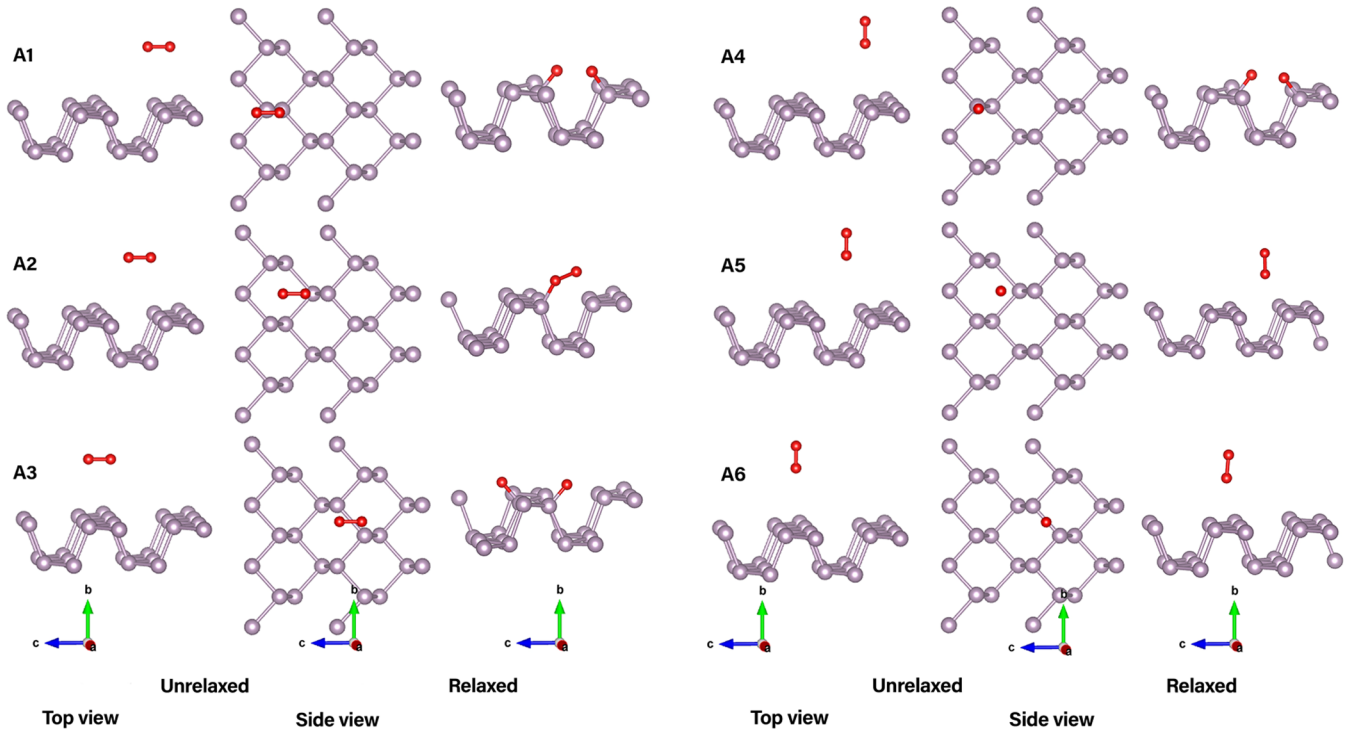

Figure 2. Models used to simulate the interaction between oxygen molecules and pristine phosphorene.

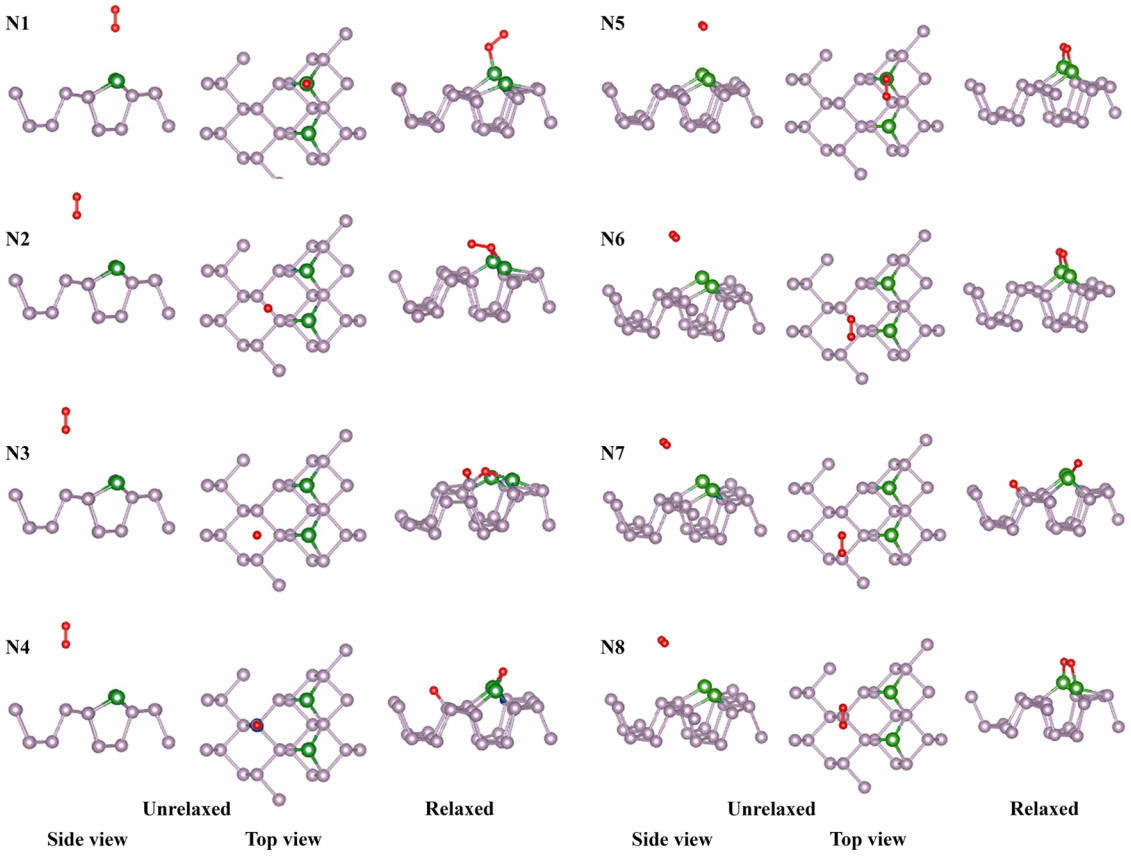

Figure 3. Models used to simulate the adsorption of oxygen molecules on nickel-loaded phosphorene.

resistance of Ni/bP. When NO_2 is introduced, the gas molecules react with nickel atoms on the surface of the layer acting as an oxidizing agent, therefore increasing the hole density. Since the electrons participating in this reaction are coming from the phosphorene layer, the result is an increase of conductance, which is discussed in detail in the Charge Transfer Analyses section. Moreover, possible adsorption processes on pristine and on nickel-decorated phosphorene were theoretically studied by

https://doi.org/10.1021/acsomega.2c00078
ACS Omega 2022, 7, 9808−9817

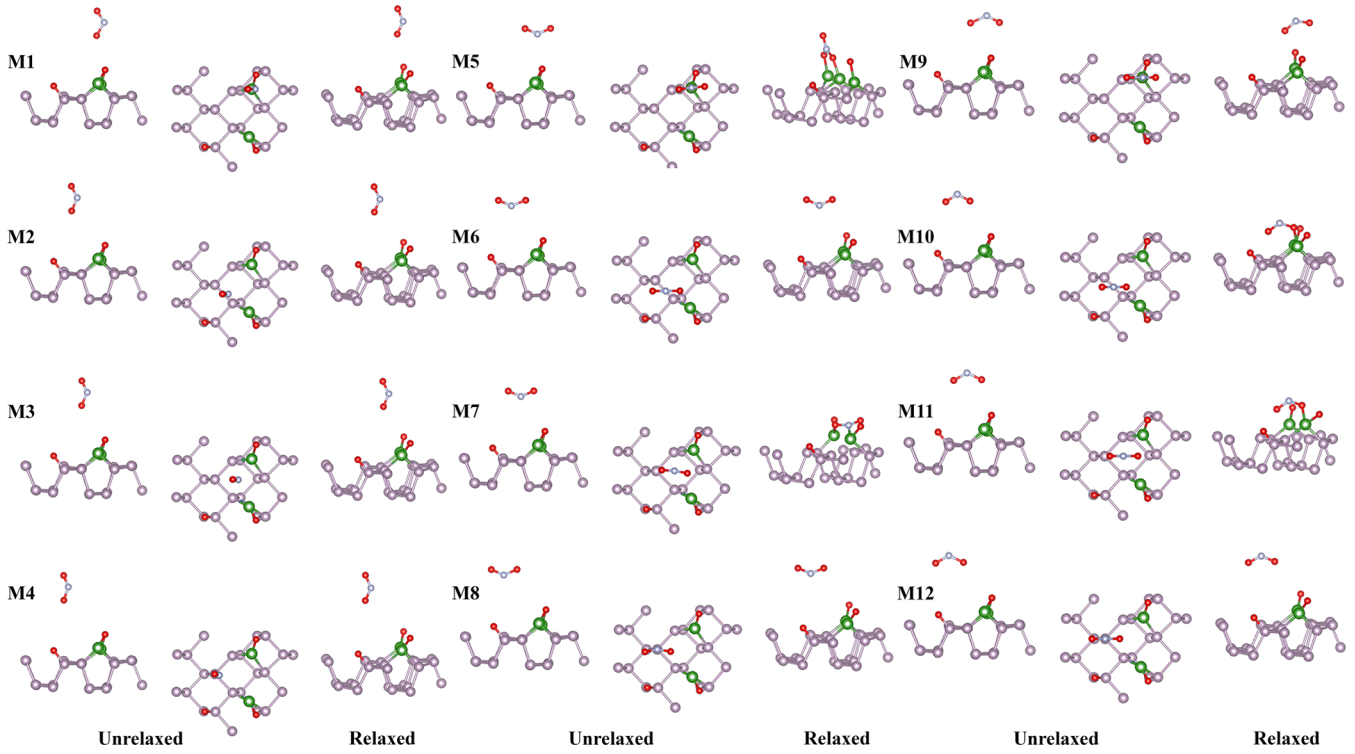

Figure 4. Models used to simulate the adsorption of NO_2 molecules on nickel-loaded phosphorene with preadsorbed oxygens.

means of DFT calculations. Finally, the charge transfer process that occurs during the reactions was considered at both stages: (i) the adsorption of oxygen molecules from the surrounding atmosphere and (ii) the interaction of NO_2 molecules with and without the preadsorbed oxygen. In Figure S4, the adsorption sites considered in this work are reported.

The sign and the value of the adsorption energy can be used to determine the probability of an adsorption mode to occur. The following eq 1 is used to calculate the adsorption energy

$$E_{ads} = E_L + E_{mol} - E_{L+mol} \quad (1)$$

where E_{L+mol} is the total energy of the relaxed system containing the layer and the molecule, E_L and E_{mol} are the energy of the relaxed layer, pristine or nickel-decorated phosphorene, and the relaxed isolated molecule (O_2 or NO_2), respectively.

On the one hand, and according to this equation, positive adsorption energy indicates that the adsorption process is exothermic and the adsorption system is thermodynamically stable. On the other hand, a negative value indicates endothermic and unstable adsorption.

Adsorption of Oxygen Species. Six models, from A1 to A6, were considered to simulate the possible interactions between oxygen molecules and the surface of pristine phosphorene. Parallel adsorptions of the O_2 molecule on the layer of phosphorene in the top (T), hollow (H), and bridge (B) sites (A1, A2, and A3 modes, respectively) and perpendicular adsorptions in the same sites (A4, A5, and A6 models, respectively) are illustrated in Figure 2. Moreover, Figure 2 shows the initial and final states of the systems after the relaxation. Table S3 summarizes the calculated adsorption energies for each model. The resulting negative adsorption energy of A2, A5, and A6 models means that the proposed reactions cannot occur (i.e., the adsorption process is endothermic, and the adsorption system is thermodynamically unstable). Instead, the calculated adsorption energies for models A1, A3, and A4 gave positive values indicating that the systems are thermodynamically stable, and the adsorption processes are exothermic or extremely exothermic (E_{ads} ~4 eV per O_2 molecule), i.e., 3.76, 3.9, and 3.76 eV, respectively. The obtained numerical results are coherent with previously reported values.[71] In addition, the results highlight that the physisorbed O_2 molecules are in a metastable state, which involves the formation of two dissociated oxygen atoms, adsorbed on the black phosphorus monolayer surface through the so-called dissociative adsorption. One can also observe that the adsorption energies for models A1 and A4 are equal, which means that the adsorption energy is not affected by the orientation of the O_2 molecule. On the contrary, the adsorption site clearly impacts on the adsorption energy, which means that the O_2 molecules cannot be adsorbed in the hollow site, whereas the bridging and top sites are preferred. In particular, the bridging site has an adsorption energy of about 3.9 eV. Such a high adsorption energy may allow the oxidation of phosphorene at room temperature, involving the degradation of the material.

For nickel-decorated phosphorene, eight models (N1−N8) were considered to investigate the adsorption of oxygen molecules on its surface (Figure 3). First, perpendicular adsorptions of the O_2 molecule on the Ni atom, B, H, and T sites were considered (case of N1, N2, N3, and N4, respectively). Then, parallel adsorptions with one atom of the oxygen molecule coordinated to the same sites, as for the perpendicular adsorption, were considered (case of N5, N6, N7, and N8). The relaxed structures are shown in Figure 3, while the adsorption energies for each model are reported in Table S4. Positive adsorption energies were obtained for all models proposed in this part, which means that the systems are thermodynamically stable, and the adsorption processes are exothermic. Investigating the values obtained for each model, it can be seen that in the case of adsorption using models N1, N2, N5, N6, and N8, the adsorption energies are lower than the

https://doi.org/10.1021/acsomega.2c00078
ACS Omega 2022, 7, 9808−9817

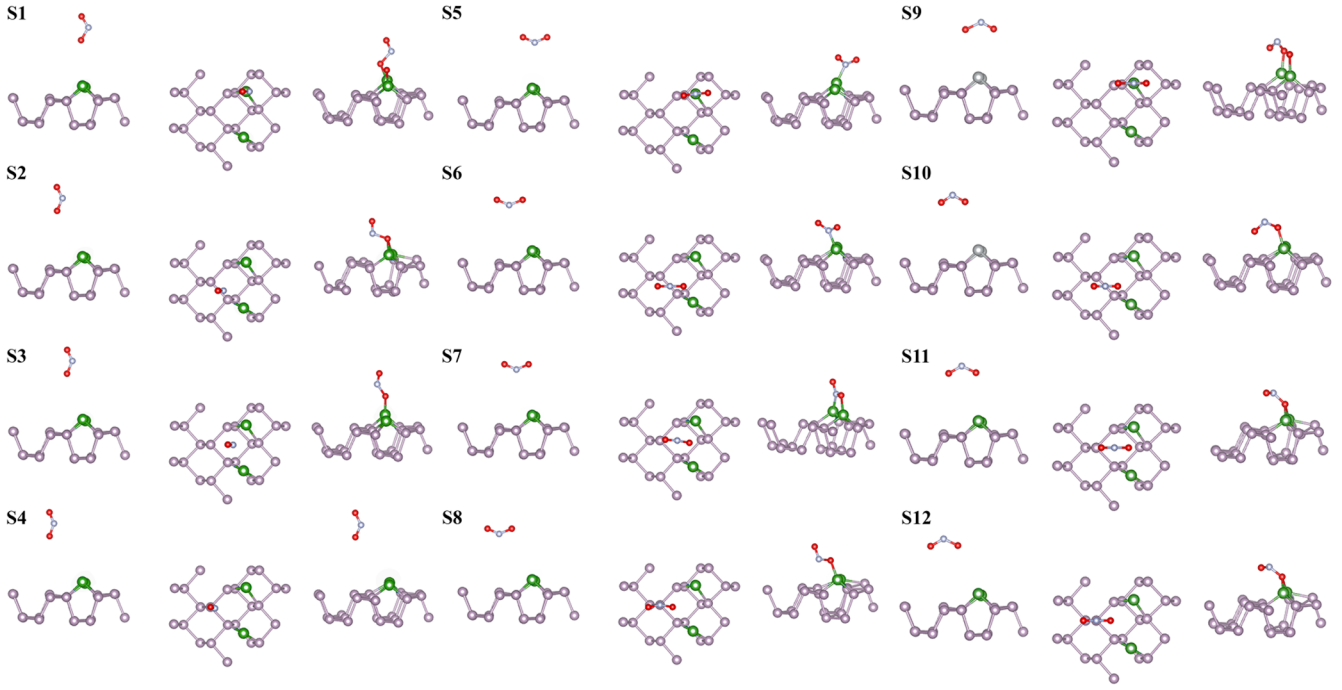

Figure 5. Models used to simulate the adsorption of NO_2 molecules on nickel-loaded phosphorene without preadsorbed oxygens.

other cases, and the oxygen molecule does not dissociate reacting only with the nickel adatoms. Otherwise, using N3, N4, and N7, the adsorption energies are higher and the oxygen molecule dissociates on the surface. Looking at the behavior of the oxygen molecule in the three models (N3, N4, and N7), it can be noticed that one O atom reacts with nickel on the surface and the other one reacts with a phosphorus atom from the layer. This may explain the improved stability and less degradation of nickel-decorated phosphorene. Indeed, by introducing nickel, some of the oxygen molecules from the surrounding atmosphere adsorb on the Ni atoms, decreasing the oxidation rate of the Ni/bP layer compared to pristine phosphorene. From Table S4, it can also be concluded that the model N7 is the most probable and stable model for the adsorption of O_2 molecules on the Ni/bP layer since it has the highest adsorption energy (E_{ads} = 3.34 eV). Discussing the interaction between oxygen and Ni atoms, we can summarize this reaction as follows: when oxygen atoms meet the Ni ones, they first take electrons and adsorb on the surface of the material. The discussion of this reaction in detail is reported later in the Charge Transfer Analyses section, where we calculated the amount of charges lost from Ni atoms as well as the one gained by oxygen atoms.

Adsorption of NO_2 Gas Molecules. To study the second stage of the sensing mechanism of Ni/bP toward NO_2 gas, two possibilities were investigated. First, the adsorption of NO_2 molecules on the layer containing the preadsorbed oxygen (model N7) was studied. Then, adsorption on the layer without preadsorbed oxygen was investigated. The second case was considered since NO_2 molecules may react with the free nickel atoms on the Ni/bP surface rather than with the preadsorbed oxygens. For this purpose, 12 models for each case (Figures 4 and 5) were considered (M1−M12 and S1−S12 for the first and the second case, respectively). In M1, M2, M3, and M4, we proposed adsorption of the NO_2 molecule in the Ni, B, H, and T sites with one oxygen atom coordinated to the adsorption site considered. Then, two other orientations of the NO_2 molecule were proposed, i.e., M5−M8 adsorption in the same sites with the N atom facing the layer, whereas for M9−M12, the oxygen atoms constituting the NO_2 molecule face the layer. The same approach was adopted for the second case but without the preadsorbed oxygens. The NO_2 molecule was placed in all cases at a starting distance of about 2.6 Å from the layer. Figure 4 displays the systems considered for the first case before and after relaxation, and the corresponding adsorption energies are summarized in Table S5. All calculated adsorption energies present positive values, resulting in the possible adsorption of the NO_2 molecule on the Ni/bP layer with the preadsorbed oxygen from the atmosphere. Analyzing the calculated adsorption energies, one can easily conclude that the NO_2 molecule might prefer the M5, M7, M10, and M11 models for its adsorption on Ni/bP, with an adsorption energy of 2.27, 1.77, 1.55, and 1.51 eV, respectively. From Figure 4, it can also be seen that using M5, M7, M10, and M11, bonds were created between the NO_2 molecule and layer, while the other models lead to NO_2 physisorption on the layer, with quite small adsorption energies (ranging from 0.25 to 0.48 eV). Another point to highlight from Figure 4 is how the NO_2 molecule establishes its bonds on the layer in the four most probable models. Indeed, the NO_2 molecule always creates its bonds with the nickel atoms at the surface regardless of its initial position. From this consideration, the need to study the adsorption of NO_2 on the layer without the preadsorbed oxygens arises. As already mentioned, the S1−S12 models shown in Figure 5 were adopted for this purpose. From the calculated adsorption energies, summarized in Table S6, it is clear that they are much higher than in the case of M models, and for the most probable case (i.e., S9 model), the calculated value was about 3 eV, which makes the process extremely exothermic and the system more stable. One can therefore conclude that the interaction of NO_2 with free nickel at the surface is more likely than with the preadsorbed oxygen on Ni atoms. At this stage, it is proposed that the sensing mechanism of Ni/bP toward NO_2 is divided into two main steps, where eq 2 stands for the

https://doi.org/10.1021/acsomega.2c00078
ACS Omega 2022, 7, 9808−9817

interaction of oxygen with the sensing layer and eq 3 for the interaction with the analyte. To confirm that, the models N7 and S9 were considered to study the charge transfer, analyzed in the next paragraph, occurring on the layer at both stages.

$$O_{2(ads)} + 2e^- \rightarrow 2O^-_{(ads)} \quad (2)$$

$$NO_{2(gas)} + e^- \rightarrow NO^-_{2(ads)} \quad (3)$$

Charge Transfer Analyses. Löwdin charge analysis models[72] were used to study the charge transfer occurring on the surface of the sensing film. Projecting the density of states on the atomic orbitals, more precisely, on angular momentum channels, which are present in the corresponding pseudopotentials, the Löwdin charges can be calculated only on the valence charge density. Hence, using the Löwdin charges, it is possible to calculate the differences between the charge values of atoms composing the system before and after interactions. The obtained trends generally correspond to the correct trends of charge transfer. In other words, relative trends are usually physically sensitive for most methods and systems including the Löwdin method that can only qualitatively estimate what is happening to the interacting molecule, and the trend is generally in agreement with experiments.[73] In our case, when the oxygen molecule is adsorbed on the surface layer, it withdraws electrons from the nickel atom gaining 1.64 |e|, meanwhile, the nickel atoms and the phosphorus layer lose 0.66 |e| and 1.0749 |e|, respectively. The number of electrons lost from the surface went to the adsorbed oxygen molecule, confirming that the reaction mentioned before (eq 2) for the first stage of the sensing mechanism of nickel-loaded phosphorene can occur. Indeed, before the interaction with the molecule, the total charge of phosphorus and nickel atoms constituting the layer was 79.1 |e| and 19.4 |e|, respectively. While after the interaction, the total charge of phosphorus and Ni atoms was 78.02 |e| and 18.74 |e|, respectively. The electrons involved in these reactions accumulate at the surface and decrease their density in the Ni/bP layer, which results in the creation of a depletion zone. By studying the charge transfer occurring during the interaction reported in the model S9, the proposed reaction in eq 3 can be confirmed, where the NO_2 molecule is adsorbed on the surface of Ni/bP and oxidized the sensing material. In other words, during the interaction, the NO_2 molecule gains 0.57 |e|, which is coming from Ni atoms since the latter are losing 0.38 |e|, meanwhile, the phosphorus atoms composing the layer lose 0.16 |e|. This means that the mechanism involved in this reaction is the Fermi level control mechanism[74] (see Figure 6). In this mechanism, the nickel atoms are partially oxidized and the phosphorus layer loses electrons, causing an increase in the hole density in the material. This results in an increase of the conductance of the sensing material, which is transduced to Ni/bP sensing response.

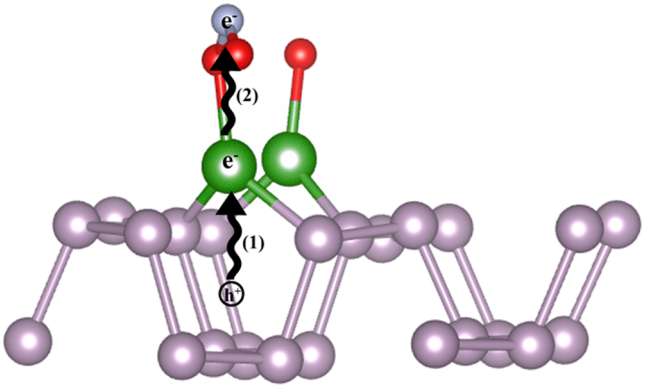

Figure 6. Mechanism involved in the interaction between the NO_2 gas molecule and nickel-decorated phosphorene (the Fermi level control mechanism). Electrons are going from the P atoms to Ni atoms leaving holes (step 1) and then going to NO_2 molecules (step 2).

CONCLUSIONS

The impact of nickel decoration on the physical−chemical properties of phosphorene and the gas sensing mechanism of the material toward the NO_2 molecule was theoretically investigated using ab initio calculations and applying DFT.

The results showed that, by introducing Ni atoms, the value of the material band gap decreased due to the new energy level created below the Fermi level. This new energy level behaves as a shallow acceptor level since it is located between the top of the VB and the Fermi level. This decrease in the band gap may enhance the sensitivity and the response time of the produced sensors. The motivation of this phenomenon lies in the carrier mobility of the sensing material, which plays a crucial role to improve the sensing performance of the final device. Indeed, in our case, when nickel is introduced in phosphorene, it captures electrons from the sensing layer as an acceptor, enriching the quantity of adsorbed oxygen and consequently enhancing the carrier mobility in the material. Exchanging electrons with environmental oxygen and NO_2 molecules, the electron depletion region changes significantly obtaining a variation in the film resistance, thus enhancing the performance of the sensing material compared to pristine phosphorene.

Furthermore, a proposed explanation of the ambient stability[49] of Ni/bP was given, i.e., decreasing the band gap and the work function of the material may lead to a decrease of the CBM below the redox potential of O_2/O_2^-, limiting in this way the production of excitons under ambient light. Indeed, this results in enhanced ambient stability and lower degradability of the material as already demonstrated experimentally.

Finally, charge transfer analysis was carried out to theoretically explain the sensing mechanism of Ni-decorated phosphorene toward the NO_2 molecule. The results revealed that the mechanism involved in this interaction is led by the Fermi level control mechanism. This would involve the electron transfer between the nickel additive and the phosphorene layer. Therefore, nickel is oxidized by the oxygen species from the surrounding atmosphere and in turn accepts electrons from the sensing layer creating a depletion zone. In conclusion, the theoretical investigation proposed here has elucidated the role of nickel decoration on the stability of phosphorene-based sensors in the NO_2 detection mechanism, which was previously observed in our experimental study. With a deep understanding of the phenomenological aspects behind the sensing material functionality, it is possible to lean toward optimization of its features as a function of the application field.

ASSOCIATED CONTENT

Supporting Information

The Supporting Information is available free of charge at https://pubs.acs.org/doi/10.1021/acsomega.2c00078.

Detailed description of the optimization processes and the approaches used for the simulation as well as the obtained adsorption energies for the considered configurations (PDF)

https://doi.org/10.1021/acsomega.2c00078
ACS Omega 2022, 7, 9808−9817

AUTHOR INFORMATION

Corresponding Authors

Soufiane Krik − *Department of Physics and Earth Sciences, University of Ferrara, 44122 Ferrara, Italy; Sensing Technologies Lab, Faculty of Science and Technology, Free University of Bozen-Bolzano, 39100 Bolzano, Italy;* Present Address: The work was conducted at Department of Physics and Earth Sciences, University of Ferrara, but the current author's affiliation is the Faculty of Science and Technology, Free University of Bozen-Bolzano; orcid.org/0000-0002-3986-5066; Email: soufiane.krik@unibz.it

Barbara Fabbri − *Department of Physics and Earth Sciences, University of Ferrara, 44122 Ferrara, Italy;* orcid.org/0000-0002-0188-2178; Email: barbara.fabbri@unife.it

Authors

Matteo Valt − *MNF − Micro Nano Facility Unit, Sensors and Devices Center, Bruno Kessler Foundation, 38123 Trento, Italy;* orcid.org/0000-0003-2621-5555

Andrea Gaiardo − *MNF − Micro Nano Facility Unit, Sensors and Devices Center, Bruno Kessler Foundation, 38123 Trento, Italy;* orcid.org/0000-0002-6688-6161

Elena Spagnoli − *Department of Physics and Earth Sciences, University of Ferrara, 44122 Ferrara, Italy;* orcid.org/0000-0002-2388-1096

Maria Caporali − *CNR ICCOM − Italian National Council for Research-Institute for the Chemistry of OrganoMetallic Compounds, 50019 Sesto Fiorentino, Italy;* orcid.org/0000-0001-6994-7313

Cesare Malagù − *Department of Physics and Earth Sciences, University of Ferrara, 44122 Ferrara, Italy*

Pierluigi Bellutti − *MNF − Micro Nano Facility Unit, Sensors and Devices Center, Bruno Kessler Foundation, 38123 Trento, Italy*

Vincenzo Guidi − *Department of Physics and Earth Sciences, University of Ferrara, 44122 Ferrara, Italy*

Complete contact information is available at: https://pubs.acs.org/10.1021/acsomega.2c00078

Author Contributions

S.K. contributed to conceptualization, methodology, formal analysis, validation, and writing—original draft. M.V. contributed to conceptualization, methodology, validation and writing—original draft. A.G. contributed to methodology, validation, writing (review and editing), and supervised the work. B.F. contributed to methodology, validation, and writing (review and editing). E.S. contributed to methodology, validation and writing—original draft. M.C. contributed to conceptualization, methodology, validation, and writing (review and editing). C.M. contributed to data curation and supervision. P.B. contributed to the validation, writing (review and editing), and funding acquisition. V.G. supervised the work and funding acquisition.

Notes

The authors declare no competing financial interest.

ACKNOWLEDGMENTS

The authors acknowledge the CINECA for the availability of high-performance computing resources and support. The authors also thank Italian Ministry of University and Research for funding the project PRIN 2017 KFY7XF FERMAT "Fast ElectRon dynamics in novel hybrid-2D MATerials".

REFERENCES

(1) Novoselov, K. S.; Geim, A. K.; Morozov, S. V.; Jiang, D.; Zhang, Y.; Dubonos, S. V.; Grigorieva, I. V.; Firsov, A. A. Electric Field in Atomically Thin Carbon Films. *Science* **2004**, *306*, 666−669.

(2) Zhang, Y.; Tang, T. T.; Girit, C.; Hao, Z.; Martin, M. C.; Zettl, A.; Crommie, M. F.; Shen, Y. R.; Wang, F. Direct Observation of a Widely Tunable Bandgap in Bilayer Graphene. *Nature* **2009**, *459*, 820−823.

(3) Rao, C. N. R.; Matte, H. S. S. R.; Subrahmanyam, K. S. Synthesis and Selected Properties of Graphene and Graphene Mimics. *Acc. Chem. Res.* **2013**, *46*, 149−159.

(4) Li, W.; Chen, B.; Meng, C.; Fang, W.; Xiao, Y.; Li, X.; Hu, Z.; Xu, Y.; Tong, L.; Wang, H.; Liu, W.; Bao, J.; Shen, Y. R. Ultrafast All-Optical Graphene Modulator. *Nano Lett.* **2014**, *14*, 955−959.

(5) Kong, X.; Liu, Q.; Zhang, C.; Peng, Z.; Chen, Q. Elemental Two-Dimensional Nanosheets beyond Graphene. *Chem. Soc. Rev.* **2017**, *46*, 2127−2157.

(6) Lei, W.; Liu, G.; Zhang, J.; Liu, M. Black Phosphorus Nanostructures: Recent Advances in Hybridization, Doping and Functionalization. *Chem. Soc. Rev.* **2017**, *46*, 3492−3509.

(7) Liu, H.; Du, Y.; Deng, Y.; Ye, P. D. Semiconducting Black Phosphorus: Synthesis, Transport Properties and Electronic Applications. *Chem. Soc. Rev.* **2015**, *44*, 2732−2743.

(8) Franklin, A. D. Nanomaterials in Transistors: From High-Performance to Thin-Film Applications. *Science* **2015**, *349*, No. aab2750.

(9) Akhtar, M.; Anderson, G.; Zhao, R.; Alruqi, A.; Mroczkowska, J. E.; Sumanasekera, G.; Jasinski, J. B. Recent Advances in Synthesis, Properties, and Applications of Phosphorene. *npj 2D Mater. Appl.* **2017**, *1*, No. 5.

(10) Anasori, B.; Lukatskaya, M. R.; Gogotsi, Y. 2D Metal Carbides and Nitrides (MXenes) for Energy Storage. *Nat. Rev. Mater.* **2017**, *2*, No. 16098.

(11) Guo, Y.; Xu, K.; Wu, C.; Zhao, J.; Xie, Y. Surface Chemical-Modification for Engineering the Intrinsic Physical Properties of Inorganic Two-Dimensional Nanomaterials. *Chem. Soc. Rev.* **2015**, *44*, 637−646.

(12) Zeng, H.; Cui, X. An Optical Spectroscopic Study on Two-Dimensional Group-VI Transition Metal Dichalcogenides. *Chem. Soc. Rev.* **2015**, *44*, 2629−2642.

(13) Tan, C.; Cao, X.; Wu, X. J.; He, Q.; Yang, J.; Zhang, X.; Chen, J.; Zhao, W.; Han, S.; Nam, G. H.; Sindoro, M.; Zhang, H. Recent Advances in Ultrathin Two-Dimensional Nanomaterials. *Chem. Rev.* **2017**, *117*, 6225−6331.

(14) Chhowalla, M.; Jena, D.; Zhang, H. Two-Dimensional Semiconductors for Transistors. *Nat. Rev. Mater.* **2016**, *1*, No. 16052.

(15) Cui, S.; Pu, H.; Wells, S. A.; Wen, Z.; Mao, S.; Chang, J.; Hersam, M. C.; Chen, J. Ultrahigh Sensitivity and Layer-Dependent Sensing Performance of Phosphorene-Based Gas Sensors. *Nat. Commun.* **2015**, *6*, No. 8632.

(16) Abbas, A. N.; Liu, B.; Chen, L.; Ma, Y.; Cong, S.; Aroonyadet, N.; Köpf, M.; Nilges, T.; Zhou, C. Black Phosphorus Gas Sensors. *ACS Nano* **2015**, *9*, 5618−5624.

(17) Cho, S.-Y.; Lee, Y.; Koh, H.-J.; Jung, H.; Kim, J.-S.; Yoo, H.-W.; Kim, J.; Jung, H.-T. Superior Chemical Sensing Performance of Black Phosphorus: Comparison with MoS_2 and Graphene. *Adv. Mater.* **2016**, *28*, 7020−7028.

(18) Mayorga-Martinez, C. C.; Sofer, Z.; Pumera, M. Layered Black Phosphorus as a Selective Vapor Sensor. *Angew. Chem., Int. Ed.* **2015**, *54*, 14317−14320.

(19) Valt, M.; Fabbri, B.; Gaiardo, A.; Gherardi, S.; Casotti, D.; Cruciani, G.; Pepponi, G.; Vanzetti, L.; Iacob, E.; Malagù, C.; Bellutti, P.; Guidi, V. Aza-Crown-Ether Functionalized Graphene Oxide for Gas Sensing and Cation Trapping Applications. *Mater. Res. Express* **2019**, *6*, No. 075603.

(20) Novel, D.; Ghio, S.; Gaiardo, A.; Picciotto, A.; Guidi, V.; Speranza, G.; Boscardin, M.; Bellutti, P.; Pugno, N. M. Strengthening of

https://doi.org/10.1021/acsomega.2c00078
ACS Omega 2022, 7, 9808−9817

Wood-like Materials via Densification and Nanoparticle Intercalation. *Nanomaterials* **2020**, *10*, No. 478.
(21) Krik, S.; Gaiardo, A.; Valt, M.; Fabbri, B.; Malagù, C.; Pepponi, G.; Bellutti, P.; Guidi, V. First-Principles Study of Electronic Conductivity, Structural and Electronic Properties of Oxygen-Vacancy-Defected SnO_2. *J. Nanosci. Nanotechnol.* **2021**, *21*, 2633−2640.
(22) Krik, S.; Gaiardo, A.; Valt, M.; Fabbri, B.; Malagù, C.; Pepponi, G.; Casotti, D.; Cruciani, G.; Guidi, V.; Bellutti, P. Influence of Oxygen Vacancies in Gas Sensors Based on Metal-Oxide Semiconductors: A First-Principles Study. In *Sensors and Microsystems*; Springer: Cham, 2020; pp 309−314.
(23) Zonta, G.; Astolfi, M.; Casotti, D.; Cruciani, G.; Fabbri, B.; Gaiardo, A.; Gherardi, S.; Guidi, V.; Landini, N.; Valt, M.; Malagù, C. Reproducibility Tests with Zinc Oxide Thick-Film Sensors. *Ceram. Int.* **2020**, *46*, 6847−6855.
(24) Gaiardo, A.; Fabbri, B.; Giberti, A.; Guidi, V.; Bellutti, P.; Malagù, C.; Valt, M.; Pepponi, G.; Gherardi, S.; Zonta, G.; Martucci, A.; Sturaro, M.; Landini, N. ZnO and Au/ZnO Thin Films: Room-Temperature Chemoresistive Properties for Gas Sensing Applications. *Sens. Actuators, B* **2016**, *237*, 1085−1094.
(25) Bagolini, A.; Gaiardo, A.; Crivellari, M.; Demenev, E.; Bartali, R.; Picciotto, A.; Valt, M.; Ficorella, F.; Guidi, V.; Bellutti, P. Development of MEMS MOS Gas Sensors with CMOS Compatible PECVD Inter-Metal Passivation. *Sens. Actuators, B* **2019**, *292*, 225−232.
(26) Spagnoli, E.; Krik, S.; Fabbri, B.; Valt, M.; Ardit, M.; Gaiardo, A.; Vanzetti, L.; Della Ciana, M.; Cristino, V.; Vola, G.; Caramori, S.; Malagù, C.; Guidi, V. Development and Characterization of WO_3 Nanoflakes for Selective Ethanol Sensing. *Sens. Actuators, B* **2021**, *347*, No. 130593.
(27) Gaiardo, A.; Zonta, G.; Gherardi, S.; Malagù, C.; Fabbri, B.; Valt, M.; Vanzetti, L.; Landini, N.; Casotti, D.; Cruciani, G.; Della Ciana, M.; Guidi, V. Nanostructured $SmFeO_3$ Gas Sensors: Investigation of the Gas Sensing Performance Reproducibility for Colorectal Cancer Screening. *Sensors* **2020**, *20*, No. 5910.
(28) Zonta, G.; Anania, G.; Astolfi, M.; Feo, C.; Gaiardo, A.; Gherardi, S.; Giberti, A.; Guidi, V.; Landini, N.; Palmonari, C.; et al. Chemoresistive Sensors for Colorectal Cancer Preventive Screening through Fecal Odor: Double-Blind Approach. *Sens. Actuators, B* **2019**, *301*, No. 127062.
(29) Fabbri, B.; Valt, M.; Parretta, C.; Gherardi, S.; Gaiardo, A.; Malagù, C.; Mantovani, F.; Strati, V.; Guidi, V. Correlation of Gaseous Emissions to Water Stress in Tomato and Maize Crops: From Field to Laboratory and Back. *Sens. Actuators, B* **2020**, *303*, No. 127227.
(30) Tran, V.; Soklaski, R.; Liang, Y.; Yang, L. Layer-Controlled Band Gap and Anisotropic Excitons in Few-Layer Black Phosphorus. *Phys. Rev. B* **2014**, *89*, No. 235319.
(31) Zhang, H.; Hu, W.; Du, A.; Lu, X.; Zhang, Y.; Zhou, J.; Lin, X.; Tang, Y. Doped Phosphorene for Hydrogen Capture: A DFT Study. *Appl. Surf. Sci.* **2018**, *433*, 249−255.
(32) Zhang, S.; Guo, S.; Chen, Z.; Wang, Y.; Gao, H.; Gómez-Herrero, J.; Ares, P.; Zamora, F.; Zhu, Z.; Zeng, H. Recent Progress in 2D Group-VA Semiconductors: From Theory to Experiment. *Chem. Soc. Rev.* **2018**, *47*, 982−1021.
(33) Li, L.; Yu, Y.; Ye, G. J.; Ge, Q.; Ou, X.; Wu, H.; Feng, D.; Chen, X. H.; Zhang, Y. Black Phosphorus Field-Effect Transistors. *Nat. Nanotechnol.* **2014**, *9*, 372−377.
(34) Liu, H.; Neal, A. T.; Zhu, Z.; Luo, Z.; Xu, X.; Tománek, D.; Ye, P. D. Phosphorene: An Unexplored 2D Semiconductor with a High Hole Mobility. *ACS Nano* **2014**, *8*, 4033−4041.
(35) Wang, Y.; Zhou, Y.; Wang, Y.; Zhang, R.; Li, J.; Li, X.; Zang, Z. Conductometric Room Temperature Ammonia Sensors Based on Titanium Dioxide Nanoparticles Decorated Thin Black Phosphorus Nanosheets. *Sens. Actuators, B* **2021**, *349*, No. 130770.
(36) Wang, Y.; Zhou, Y.; Ren, H.; Wang, Y.; Zhu, X.; Guo, Y.; Li, X. Room-Temperature and Humidity-Resistant Trace Nitrogen Dioxide Sensing of Few-Layer Black Phosphorus Nanosheet by Incorporating Zinc Oxide Nanowire. *Anal. Chem.* **2020**, *92*, 11007−11017.
(37) Cho, S.-Y.; Koh, H.-J.; Yoo, H.-W.; Jung, H.-T. Tunable Chemical Sensing Performance of Black Phosphorus by Controlled Functionalization with Noble Metals. *Chem. Mater.* **2017**, *29*, 7197−7205.
(38) Ren, H.; Zhou, Y.; Wang, Y.; Zhu, X.; Gao, C.; Guo, Y. Improving Room-Temperature Trace NO_2 Sensing of Black Phosphorus Nanosheets by Incorporating Benzyl Viologen. *Sens. Actuators, B* **2020**, *321*, No. 128520.
(39) Han, B.; Duan, Z.; Xu, J.; Zhu, Y.; Xu, Q.; Wang, H.; Tai, H.; Weng, J.; Zhao, Y. The Art of Integrated Functionalization: Super Stable Black Phosphorus Achieved through Metal-Organic Framework Coating. *Adv. Funct. Mater.* **2020**, *30*, No. 2002232.
(40) Lalitha, M.; Nataraj, Y.; Lakshmipathi, S. Calcium Decorated and Doped Phosphorene for Gas Adsorption. *Appl. Surf. Sci.* **2016**, *377*, 311−323.
(41) Li, Q. F.; Wan, X. G.; Duan, C. G.; Kuo, J. L. Theoretical Prediction of Hydrogen Storage on Li-Decorated Monolayer Black Phosphorus. *J. Phys. D: Appl. Phys.* **2014**, *47*, No. 465302.
(42) Caporali, M.; Serrano-Ruiz, M.; Telesio, F.; Heun, S.; Verdini, A.; Cossaro, A.; Dalmiglio, M.; Goldoni, A.; Peruzzini, M. Enhanced Ambient Stability of Exfoliated Black Phosphorus by Passivation with Nickel Nanoparticles. *Nanotechnology* **2020**, *31*, No. 275708.
(43) Li, G.; Wang, X.; Ding, H.; Zhang, T. A Facile Synthesis Method for Ni (OH) 2 Ultrathin Nanosheets and Their Conversion to Porous NiO Nanosheets Used for Formaldehyde Sensing. *RSC Adv.* **2012**, *2*, 13018−13023.
(44) Lin, Z.; Li, N.; Chen, Z.; Fu, P. The Effect of Ni Doping Concentration on the Gas Sensing Properties of Ni Doped SnO2. *Sens. Actuators, B* **2017**, *239*, 501−510.
(45) Bao, M.; Chen, Y.; Li, F.; Ma, J.; Lv, T.; Tang, Y.; Chen, L.; Xu, Z.; Wang, T. Plate-like p−n Heterogeneous NiO/WO_3 Nanocomposites for High Performance Room Temperature NO_2 Sensors. *Nanoscale* **2014**, *6*, 4063−4066.
(46) Yang, Y.; Wang, H.; Wang, L.; Ge, Y.; Kan, K.; Shi, K.; Chen, J. A Novel Gas Sensor Based on Porous α-Ni (OH) 2 Ultrathin Nanosheet/Reduced Graphene Oxide Composites for Room Temperature Detection of NO X. *New J. Chem.* **2016**, *40*, 4678−4686.
(47) Kulish, V. V.; Malyi, O. I.; Persson, C.; Wu, P. Adsorption of Metal Adatoms on Single-Layer Phosphorene. *Phys. Chem. Chem. Phys.* **2015**, *17*, 992−1000.
(48) Valencia, H.; Gil, A.; Frapper, G. Trends in the Adsorption of 3d Transition Metal Atoms onto Graphene and Nanotube Surfaces: A DFT Study and Molecular Orbital Analysis. *J. Phys. Chem. C* **2010**, *114*, 14141−14153.
(49) Valt, M.; Caporali, M.; Fabbri, B.; Gaiardo, A.; Krik, S.; Iacob, E.; Vanzetti, L.; Malagù, C.; Banchelli, M.; D'Andrea, C.; Serrano-Ruiz, M.; Vanni, M.; Peruzzini, M.; Guidi, V. Air Stable Nickel-Decorated Black Phosphorus and Its Room-Temperature Chemiresistive Gas Sensor Capabilities. *ACS Appl. Mater. Interfaces* **2021**, *13*, 44711−44722.
(50) Molaei, M.; Alipour, S.; Targholi, E.; Farahati, R.; Mousavi-Khoshdel, S. M. Computational Study of H_2S Adsorption on the Pristine and Transitional Metal-Doped Phosphorene. *J. Mol. Model.* **2021**, *27*, No. 181.
(51) Zhang, J.; Hong, Y.; Liu, M.; Yue, Y.; Xiong, Q.; Lorenzini, G. Molecular Dynamics Simulation of the Interfacial Thermal Resistance between Phosphorene and Silicon Substrate. *Int. J. Heat Mass Transfer* **2017**, *104*, 871−877.
(52) Chen, X.; Wu, Y.; Wu, Z.; Han, Y.; Xu, S.; Wang, L.; Ye, W.; Han, T.; He, Y.; Cai, Y.; Wang, N. High-Quality Sandwiched Black Phosphorus Heterostructure and Its Quantum Oscillations. *Nat. Commun.* **2015**, *6*, No. 7315.
(53) Kou, L.; Frauenheim, T.; Chen, C. Phosphorene as a Superior Gas Sensor: Selective Adsorption and Distinct I−V Response. *J. Phys. Chem. Lett.* **2014**, *5*, 2675−2681.
(54) Tang, X.; Du, A.; Kou, L. Gas Sensing and Capturing Based on Two-dimensional Layered Materials: Overview from Theoretical Perspective. *Wiley Interdiscip. Rev. Comput. Mol. Sci.* **2018**, *8*, No. e1361.
(55) Slater, J. C. Wave Functions in a Periodic Potential. *Phys. Rev.* **1937**, *51*, 846−851.

https://doi.org/10.1021/acsomega.2c00078
ACS Omega 2022, 7, 9808−9817

(56) Kohn, W.; Sham, L. J. Self-Consistent Equations Including Exchange and Correlation Effects. *Phys. Rev.* **1965**, *140*, No. A1133.
(57) Giannozzi, P.; Baseggio, O.; Bonfà, P.; Brunato, D.; Car, R.; Carnimeo, I.; Cavazzoni, C.; De Gironcoli, S.; Delugas, P.; Ferrari Ruffino, F.; Ferretti, A.; Marzari, N.; Timrov, I.; Urru, A.; Baroni, S. Quantum ESPRESSO toward the Exascale. *J. Chem. Phys.* **2020**, *152*, No. 154105.
(58) Perdew, J. P.; Burke, S.; Ernzerhof, M. The Exchange-Correlation Potential in the GGA Approximation. *Phys. Rev. Lett.* **1996**, *77*, 3865−3868.
(59) Pack, J. D.; Monkhorst, H. J. "special Points for Brillouin-Zone Integrations"-a Reply. *Phys. Rev. B* **1977**, *16*, 1748−1749.
(60) Witzgall, C.; Fletcher, R. *Practical Methods of Optimization*; John Wiley & Sons, 1989; Vol. *53*.
(61) Klimeš, J.; Bowler, D. R.; Michaelides, A. Chemical Accuracy for the van Der Waals Density Functional. *J. Phys.: Condens. Matter* **2010**, *22*, No. 022201.
(62) Klime, J.; Bowler, D. R.; Michaelides, A. Van Der Waals Density Functionals Applied to Solids. *Phys. Rev. B* **2011**, *83*, No. 195131.
(63) Hu, T.; Hong, J. First-Principles Study of Metal Adatom Adsorption on Black Phosphorene. *J. Phys. Chem. C* **2015**, *119*, 8199−8207.
(64) Liu, X.; Chen, K.; Li, X.; Xu, Q.; Weng, J.; Xu, J. Electron Matters: Recent Advances in Passivation and Applications of Black Phosphorus. *Adv. Mater.* **2021**, *33*, No. 2005924.
(65) Zhang, R.; Li, B.; Yang, J. A First-Principles Study on Electron Donor and Acceptor Molecules Adsorbed on Phosphorene. *J. Phys. Chem. C* **2015**, *119*, 2871−2878.
(66) Cai, Y.; Zhang, G.; Zhang, Y.-W. Layer-Dependent Band Alignment and Work Function of Few-Layer Phosphorene. *Sci. Rep.* **2015**, *4*, No. 6677.
(67) Dufek, P.; Blaha, P.; Schwarz, K. Applications of Engel and Voskos Generalized Gradient Approximation in Solids. *Phys. Rev. B* **1994**, *50*, 7279−7283.
(68) Peralta, J. E.; Heyd, J.; Scuseria, G. E.; Martin, R. L. Spin-Orbit Splittings and Energy Band Gaps Calculated with the Heyd-Scuseria-Ernzerhof Screened Hybrid Functional. *Phys. Rev. B* **2006**, *74*, No. 174101.
(69) Zhou, Q.; Chen, Q.; Tong, Y.; Wang, J. Light-Induced Ambient Degradation of Few-Layer Black Phosphorus: Mechanism and Protection. *Angew. Chem., Int. Ed.* **2016**, *55*, 11437−11441.
(70) Barsan, N.; Koziej, D.; Weimar, U. Metal Oxide-Based Gas Sensor Research: How To? *Sens. Actuators, B* **2007**, *121*, 18−35.
(71) Huang, Y.; Qiao, J.; He, K.; Bliznakov, S.; Sutter, E.; Chen, X.; Luo, D.; Meng, F.; Su, D.; Decker, J.; et al. Interaction of Black Phosphorus with Oxygen and Water. *Chem. Mater.* **2016**, *28*, 8330−8339.
(72) Löwdin, P. On the Non-Orthogonality Problem Connected with the Use of Atomic Wave Functions in the Theory of Molecules and Crystals. *J. Chem. Phys.* **1950**, *18*, 365−375.
(73) Reed, A. E.; Weinstock, R. B.; Weinhold, F. Natural Population Analysis. *J. Chem. Phys.* **1985**, *83*, 735−746.
(74) Yamazoe, N. New Approaches for Improving Semiconductor Gas Sensors. *Sens. Actuators, B* **1991**, *5*, 7−19.

https://doi.org/10.1021/acsomega.2c00078
ACS Omega 2022, 7, 9808−9817